Int J Adv Manuf Technol (2015) 78:895–905
DOI 10.1007/s00170-014-6675-9

ORIGINAL ARTICLE

Influence of additional tensile force on the stress and deformation of numerically controlled tube bending

Daxin E. · Rongting Li

Received: 26 April 2014 / Accepted: 1 December 2014 / Published online: 19 December 2014

Abstract According to the working way of the numerically controlled (NC) tube bender and taking the additional tensile force into account, the formulas are derived to calculate the average principal stress in different directions of the bending tube surface, the equivalent stress, the variation of wall thickness, and the ratio of the minor axis to the original radius of outer contour and validated by the experiments. The corresponding experiments and simulation analysis are performed to compare with the calculated results, and it is revealed that the equivalent stress of the bending tube surface is non-uniform and the maximum equivalent stress is localized in smaller deformation field around the bending terminating end. The consideration of the additional tensile force makes the equivalent stress in the outer convex portion of tube remarkably greater than that in the inner concave portion of tube, accelerating the thinning of the tube's wall and the ovalization of tube's outer contour. The approximate calculation formulae of additional tensile force is also derived and based on the deformation analysis; the proper adjustment of the additional tensile force could improve the quality of the NC bending tube.

Keywords NC bending · Additional tensile force · Equivalent stress · Wall thinning · Cross-sectional ovalization

D. E. · R. Li
School of Materials Science and Engineering, Beijing Institute of Technology, Beijing 100081, People's Republic of China

D. E. (✉)
N0.5, South Street of Zhongguancun, Haidian District, Beijing, People's Republic of China
e-mail: daxine@bit.edu.cn

1 Induction

The numerically controlled (NC) bending is an important method to develop an accurate bending technology, but technical problems still exist due to the limitations of the bending theory. Studies from different perspective have been widely carried out to study the tube bending [1–7].

Oliveira [8] analyzed the thickness and strain distributions within the aluminum alloy s-rail by experiments and finite element simulations, revealing that the bending degree had the most significant effect on the variation of wall thickness variation and the strain distribution. Meanwhile the "boost" in bending aggravated the variation of wall thickness and the work hardening capacity in the bend regions of the s-rail. Strano [9] developed a comprehensive computer approach for the automatic process design of rotary draw bending of tubes, named Tube ProDes. The advanced process simulated the compensation and severity of bending before the tool experiments, then with parameters obtained previously, the bending process was precisely conducted. Li et al. [10] explored the wrinkling, wall thinning, and cross-section deformation during the thin-walled tube NC bending by using a series of 3D-FE models under ABAQUS platform. The research revealed that the tangent stress increased and became more non-uniform with the Rd/D decreasing, while with larger D/t, both the wall thinning and thickening degrees increased. Zhan et al. [11] obtained the compatible range of the mandrel diameter and axial feed during the NC bending of a TA18 tube with the consideration of the influence of the equivalent mandrel supporting radius and equivalent mandrel supporting angle. Zhang et al. [12] studied about the bending behaviors of large-diameter thin-walled (LDTW) CP-Ti tube in rotary draw bending by experiments and simulation analysis, with a series of three-dimensional finite element models of the testing tube. It was revealed in the study that with the increase of the difference between the maximum wall

thickening degree and the maximum wall thinning degree of the bent tube, the wrinkling tendency became more obvious and the wrinkling was significantly influenced by the mandrel shank diameter. But, the thinning of tube wall was mainly affected by the clearance between wiper die and tube, mandrel shank diameter.

The investigations above undoubtedly promote the development of tube-bending theory and the NC tube-bending technology. However, problems concerning bending mechanism still exist and affect the actual production in certain extent. For examples, severe thinning of the tube wall and crack in actual production, which is closely related to the frictional forces in bending forming, may induce the explosion in the conveying process of high-pressure fluid now and then. While the frictional forces are always overcome by controlling the additional tensile force of bending die in NC tube bending. In the serial tests of tube bending, our preliminary work is mainly based on the plastic-bending theory. The theoretical analyses on springback and time-dependent springback of bending tube have been carried out with amount of experimental and numerical investigations [13–15]. This article is based on the working way of the NC tube bender, without regard to the difference between bend-stretch and stretch-bend. The study focuses on the analysis of the influence of the additional tensile force on the stress-train state during bending and the formability of tube. It is believed that the bending deformation is attributed to the combined action of the bending moment and the constant additional tensile force. It would provide reference for the investigation of bending mechanism and the development of NC tube-bending technology.

2 Material and methods

2.1 Bending experiments

Laser tester and numerical control (NC) VB-300HP bender were utilized in the tests. The basic schematic diagram of NC tube bending is shown in Fig. 1. During tube bending, the tube rotates the fixed axle under the combined clamping of the bending die and the clamping die. The unbent part of the tube is under restraint of the pressure die and the wiper die in the vertical direction of the feeding direction. Then, the unbent tube would enter the bending area along the feeding direction with bending deformation. Due to the sliding friction between the surface of tube wall and the grooves of the pressure die and the wiper die, a tensile force T along tangential direction of bending die should be added near the bending point to balance the frictional forces along the feeding direction. Therefore, the NC tube bending shows the properties of stretch bending in certain extent [16]. The additional tensile force T is assumed to be unchanged during bending when analyzing the stress state.

In a series of bending tests of thin-walled tubes with small diameter, the materials of tubes involve 1Cr8Ni9Ti, 5A03 (aerial corrosion-resisting aluminum), and T2 (pure copper), and their wall-thickness/diameter ratios t_0/d_0 ranged from 0.1 to 0.25. The mechanical properties of the materials from tensile tests are present in Table 1, where E is the elastic modulus, D is the linear hardening coefficient, and σ_{s0} is the original yield stress.

2.2 Finite element methods

To understand the distribution of the all principal stress along the bending line, the 3D elastic–plastic FE model for NC tube bending has been established in the eta/DYNAFORM software environment. As the complex forming process of the ratary draw bending involving large deformation, large displacement, material nonlinearity, geometry nonlinearity, and boundary condition nonlinearity. The key problems during the bending simulation, like material properties, contact conditions, and integration algorithm need to be selected precisely.

It was assumed that the tube material in the simulation was isotropic, homogeneous, and elastic–plastic. The Barlet anisotropic material model was selected as the material model. Material properties were obtained from the uniaxial tensile tests (Table 1). The thin-shell structure was selected as the meshing element and a faster calculating method BELYTSCHKO-TSAY was applied. The static and dynamic friction coefficients between the dies and the tube were, respectively, μ_s=0.15 and μ_d=0.1. The bending die speed was 10 rad/s.

3 Analysis

3.1 Stress analysis in NC tube bending

To reduce the complexity of analysis, the process of the NC tube bending is assumed to be in the plane-strain that the hoop strain of the cross-section ε_φ=0 and the tangential strain ε_θ, the radial strain ε_R, and the circumferential strain ε_φ are all principal strain. Based on the assumption that the volume is uncompressible during bending, the equation ε_θ=−ε_R is set up. The circumferential principal stress σ_φ, the tangential principal stress σ_θ, and the radial principal stress σ_R show the relationship as following:

$$\sigma_\varphi = \frac{\sigma_\theta + \sigma_R}{2} \tag{1}$$

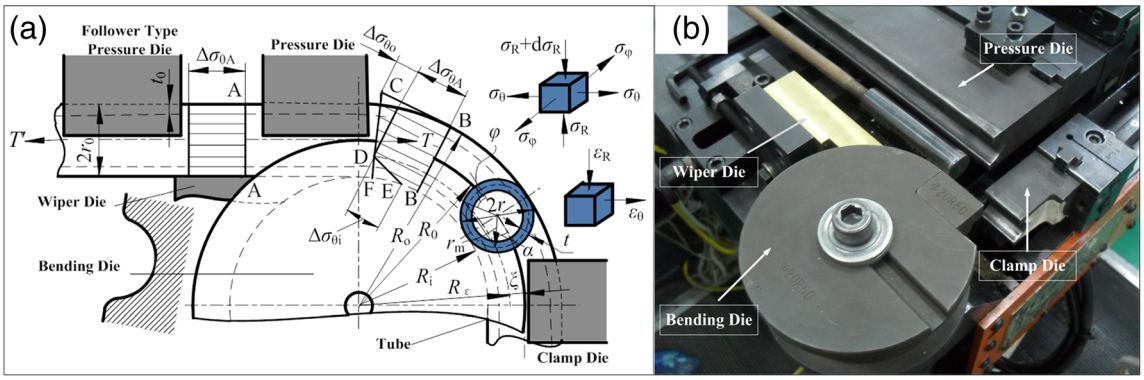

Fig. 1 The state of stress–strain and the geometric relationship of deformation in NC tube bending

The equivalent stress and the equivalent strain can be expressed as

$$\overline{\sigma} = \sqrt{\frac{1}{2}\left[(\sigma_\theta - \sigma_R)^2 + (\sigma_R - \sigma_\varphi)^2 + (\sigma_\varphi - \sigma_\theta)^2\right]} = \frac{\sqrt{3}}{2}|\sigma_\theta - \sigma_R| \quad (2)$$

$$\overline{\varepsilon} = \frac{\sqrt{2}}{3}\sqrt{(\varepsilon_\theta - \varepsilon_R)^2 + (\varepsilon_R - \varepsilon_\varphi)^2 + (\varepsilon_\varphi - \varepsilon_\theta)^2} = \frac{2}{\sqrt{3}}|\varepsilon_\theta| \quad (3)$$

Based on the state of stress–strain in Fig. 1, it is assumed that no shear deformation exists between the longitudinal fiber layers of the tube. According to the projection relationship of all principal stress in bending-plane and neglecting the second-order trace in force balance equation, we can easily obtain

$$\frac{d\sigma_R}{dR} = \frac{\sigma_\theta - \sigma_R}{R} \quad (4)$$

In view of the material hardening exponent n that may destroy the rigor of the power function integral, the material of tube is simplified as the linear hardening model. The tangential tensile force σ_T caused by the additional tensile force T, the equivalent stress, and the equivalent strain show a relation as the following:

$$\overline{\sigma} = \sigma_{s0} + \sigma_T + D\left(\overline{\varepsilon} - \varepsilon_{s0}\right) \quad (5)$$

where σ_{s0} is the initial yield stress of the tube and ε_{s0} is the corresponding initial yield strain ($\varepsilon_{s0}=\sigma_{s0}/E$, E is elastic modulus), and D is the linear hardening coefficient.

Table 1 The mechanical properties of tube materials

Material	E (GPa)	D (MPa)	σ_{s0} (MPa)
1Cr8Ni9Ti	198	1080	205
5A03	73	275	80
T2	110	411	70

The engineering strain in tangential direction of the bending can be expressed as

$$\varepsilon_\theta = \frac{r\sin\varphi + r\sin\alpha}{R_0 - r\sin\alpha} \quad (6)$$

where α is the displacement angle of the strain neutral layer (NL) and constant positive value.

Substituting Eqs. 2, 3, and 6 into Eq 5, we can obtain

$$\sigma_\theta - \sigma_R = \mp\frac{2}{\sqrt{3}}\sigma_{s0}\left(1 - \frac{D}{E}\right) + \frac{2}{\sqrt{3}}\sigma_T + D\frac{4}{3}\frac{r\sin\varphi + r\sin\alpha}{R - r\sin\alpha} \quad (7)$$

According to Eq. 7, when in interval $[0,\pi]$ and $[\pi,\pi+\alpha]$, $r\sin\varphi + r\sin\alpha > 0$, the tangential tensile deformation occurs; when in interval $[2\pi-\alpha,2\pi]$, $r\sin\varphi + r\sin\alpha < 0$, the deformation is still tangential tensile deformation and the first item on the right side of Eq. 7 selects the sign "+"; when in interval $[\pi+\alpha,2\pi-\alpha]$, $r\sin\varphi + r\sin\alpha < 0$, the tangential compressive deformation occurs and the first item on the right side of Eq. 7 selects the sign "–".

Substituting Eq. 7 into Eq. 4, we can obtain

$$d\sigma_R = (\sigma_\theta - \sigma_R)\frac{dR}{R} = \left[\pm\frac{2}{\sqrt{3}}\sigma_{s0}\left(1 - \frac{D}{E}\right) + \frac{2}{\sqrt{3}}\sigma_T + D\frac{4}{3}\frac{r\sin\varphi + r\sin\alpha}{R_0 - r\sin\alpha}\right]\frac{dR}{R} \quad (8)$$

Integrating the equation above, the following equation can be derived:

$$\sigma_{Ri} = \left[-\frac{2}{\sqrt{3}}\sigma_{s0}\left(1 - \frac{D}{E}\right) + \frac{2}{\sqrt{3}}\sigma_T + D\frac{4}{3}\frac{r\sin\varphi + r\sin\alpha}{R_0 - r\sin\alpha}\right]\ln R + C_i \quad (9)$$

$$\sigma_{Ro} = \left[\frac{2}{\sqrt{3}}\sigma_{s0}\left(1 - \frac{D}{E}\right) + \frac{2}{\sqrt{3}}\sigma_T + D\frac{4}{3}\frac{r\sin\varphi + r\sin\alpha}{R_0 - r\sin\alpha}\right]\ln R + C_o \quad (10)$$

where C_i and C_o are integration constants of the inner concave portion and the outer convex portion of the bending tube.

When $R=R_i$ or $R=R_o$, the radial principal stress is equal to zero, we could obtain the following:

$$C_i = \left[\frac{2}{\sqrt{3}}\sigma_{s0}\left(1-\frac{D}{E}\right)-\frac{2}{\sqrt{3}}\sigma_T-D\frac{4}{3}\frac{r\sin\varphi+r\sin\alpha}{R_0-r\sin\alpha}\right]\ln R_i \quad (11)$$

$$C_o = -\left[\frac{2}{\sqrt{3}}\sigma_{s0}\left(1-\frac{D}{E}\right)+\frac{2}{\sqrt{3}}\sigma_T+D\frac{4}{3}\frac{r\sin\varphi+r\sin\alpha}{R-r\sin\alpha}\right]\ln R_o \quad (12)$$

Substituting Eqs. 11 and 12 into Eqs. 9 and 10, we can obtain the radial stress of the inner concave portion and the outer convex portion of the bending tube

$$\sigma_{Ri} = \frac{2}{\sqrt{3}}\sigma_{s0}\left(1-\frac{D}{E}\right)\ln\frac{R_i}{R}+\left(\frac{2}{\sqrt{3}}\sigma_T+D\frac{4}{3}\frac{r\sin\varphi+r\sin\alpha}{R_0-r\sin\alpha}\right)\ln\frac{R}{R_i} \quad (13)$$

$$\sigma_{Ro} = \left[\frac{2}{\sqrt{3}}\sigma_{s0}\left(1-\frac{D}{E}\right)+\frac{2}{\sqrt{3}}\sigma_T+D\frac{4}{3}\frac{r\sin\varphi+r\sin\alpha}{R_0-r\sin\alpha}\right]\ln\frac{R}{R_o} \quad (14)$$

Substituting Eqs. 13 and 14 into Eq. 7, we can obtain the tangential stress in the inner concave portion and the outer convex portion of the bending tube as the following:

$$\sigma_{\theta i} = \frac{2}{\sqrt{3}}\sigma_{s0}\left(1-\frac{D}{E}\right)\left(\ln\frac{R_i}{R}-1\right)+\left(\frac{2}{\sqrt{3}}\sigma_T+D\frac{4}{3}\frac{r\sin\varphi+r\sin\alpha}{R_0-r\sin\alpha}\right)\left(1+\ln\frac{R}{R_i}\right) \quad (15)$$

$$\sigma_{\theta o} = \left[\frac{2}{\sqrt{3}}\sigma_{s0}\left(1-\frac{D}{E}\right)+\frac{2}{\sqrt{3}}\sigma_T+D\frac{4}{3}\frac{r\sin\varphi+r\sin\alpha}{R_0-r\sin\alpha}\right]\left(1+\ln\frac{R}{R_o}\right) \quad (16)$$

According to the relation in Eq. 1, the circumferential principal stress in the inner concave portion and the outer convex portion of the bending tube can be given as the following:

$$\sigma_{\varphi i} = \frac{\sigma_{s0}}{\sqrt{3}}\left(1-\frac{D}{E}\right)\left(2\ln\frac{R_i}{R}-1\right)+\left(\frac{\sigma_T}{\sqrt{3}}+D\frac{2}{3}\frac{r\sin\varphi+r\sin\alpha}{R_0-r\sin\alpha}\right)\left(1+2\ln\frac{R}{R_i}\right) \quad (17)$$

$$\sigma_{\varphi o} = \left[\frac{\sigma_{s0}}{\sqrt{3}}\left(1-\frac{D}{E}\right)+\frac{\sigma_T}{\sqrt{3}}+D\frac{4}{3}\frac{r\sin\varphi+r\sin\alpha}{R_0-r\sin\alpha}\right]\left(1+2\ln\frac{R}{R_o}\right) \quad (18)$$

In the surface of the bending tube, the radial stress σ_R is equal to zero. According to the relation in Eq. 2, the equivalent strain in the innermost concave portion and in the outermost convex portion of the bending tube could be derived as follows:

$$\overline{\sigma}_i = \left|\sigma_{s0}\left(1-\frac{D}{E}\right)\left(\ln\frac{R_i}{R}-1\right)+\left(\sigma_T+D\frac{2}{\sqrt{3}}\frac{r\sin\varphi+r\sin\alpha}{R_0-r\sin\alpha}\right)\left(1+\ln\frac{R}{R_i}\right)\right| \quad (19)$$

$$\overline{\sigma}_o = \left|\left[\sigma_{s0}\left(1-\frac{D}{E}\right)+\sigma_T+D\frac{2}{\sqrt{3}}\frac{r\sin\varphi+r\sin\alpha}{R_0-r\sin\alpha}\right]\left(1+\ln\frac{R}{R_o}\right)\right| \quad (20)$$

If the displacement of the strain neutral layer (NL) in tube bending is neglected, namely, $\alpha=0$, and when $\varphi=\pm\pi/2$, Eqs. 19 and 20 can be simplified as follows:

$$\overline{\sigma}_i = \left|\sigma_{s0}\left(1-\frac{D}{E}\right)\left(\ln\frac{2R_0/d_0-1}{2R/d_0}-1\right)+\left(\sigma_T-\frac{D}{\sqrt{3}}\frac{1}{R/d_0}\right)\left(1+\ln\frac{2R/d_0}{2R_0/d_0-1}\right)\right| \quad (19a)$$

$$\overline{\sigma}_o = \left|\left[\sigma_{s0}\left(1-\frac{D}{E}\right)+\sigma_T+\frac{D}{\sqrt{3}}\frac{1-\Delta t_o/r_0}{R_0/d_0}\right]\left(1+\ln\frac{2R/d_0}{2R_0/d_0+1-\Delta t_o/r_0}\right)\right| \quad (20a)$$

Assuming that the tangential tensile force σ_T caused by the additional tensile force T is equal to the initial yield stress of the material, namely, $\sigma_T=\sigma_{Ts0}$, Eqs. 19a and 20a would be adjusted to the following:

$$\overline{\sigma}_i = \left|2\sigma_{s0}\ln\frac{2R/d_0-1}{2R/d_0}-\frac{D}{E}\left(\ln\frac{2R/d_0-1}{2R/d_0}-1\right)-\frac{D}{\sqrt{3}}\frac{1}{R/d_0}\left(1+\ln\frac{2R/d_0}{2R/d_0-1}\right)\right| \quad (19b)$$

$$\overline{\sigma}_o = \left|\left[\sigma_{s0}\left(2-\frac{D}{E}\right)+\frac{D}{\sqrt{3}}\frac{1-\Delta t_o/r_0}{R/d_0}\right]\left(1+\ln\frac{2R/d_0}{2R/d_0+1-\Delta t_o/r_0}\right)\right| \quad (20b)$$

If the influence of the additional tensile force is neglected, namely, $\sigma_T=0$, the equation above can be simplified as follows:

$$\overline{\sigma}_i = \left|\sigma_{s0}\left(1-\frac{D}{E}\right)\left(\ln\frac{2R/d_0-1}{2R/d_0}-1\right)-\frac{D}{\sqrt{3}}\frac{1}{R/d_0}\left(1+\ln\frac{2R/d_0}{2R/d_0-1}\right)\right| \quad (19c)$$

$$\overline{\sigma}_o = \left|\left[\sigma_{s0}\left(1-\frac{D}{E}\right)+\frac{D}{\sqrt{3}}\frac{1-\Delta t_o/r_0}{R/d_0}\right]\left(1+\ln\frac{2R/d_0}{1+2R/d_0-\Delta t_o/r_0}\right)\right| \quad (20c)$$

When the thinning of the outer convex portion of the tube is neglected, the average equivalent stress of the outer convex portion of the bending tube can be given as follows:

$$\overline{\sigma}_{\mathrm{o}} = \left| \left[\sigma_{\mathrm{s0}} \left(1 - \frac{D}{E} \right) + \frac{D}{\sqrt{3}} \frac{1}{R/d_0} \right] \left(1 + \ln \frac{2R/d_0}{2R/d_0 + 1} \right) \right| \quad (20\mathrm{d})$$

3.2 Finite element analysis of the bending stress distribution

The value of stress calculated by equations above is just the average stress of the tube surface; however, the FEM results represented in Fig. 2 reveal that the equivalent stress of the bending tube surface $\overline{\sigma}$ along the circumferential direction of the bending tube and bending line direction is non-uniform. Along the circumferential direction of tube's cross-section, the maximum equivalent stress is localized at the field around the end of the minimum and the maximum bending radius. In the upper and the lower surface being parallel to the bending plane, the equivalent stress is quite small. Figure 3 describes the distribution of the maximum equivalent stress along the bending line. The result shows that the maximum equivalent stress of the innermost and the outermost of the bending tube are mainly localized at a small field near the bending angle 30° to the terminating end, and the equivalent stress in the outer convex portion of tube is remarkably greater than that in the inner concave portion of tube, namely $\overline{\sigma}_{\mathrm{o\ max}} > \overline{\sigma}_{\mathrm{i\ max}}$. For the bent portion of the tube, incompletely unloading, the maximum equivalent stress $\overline{\sigma}$ decreases rapidly when reaching the leading end. The equivalent stress of the outer

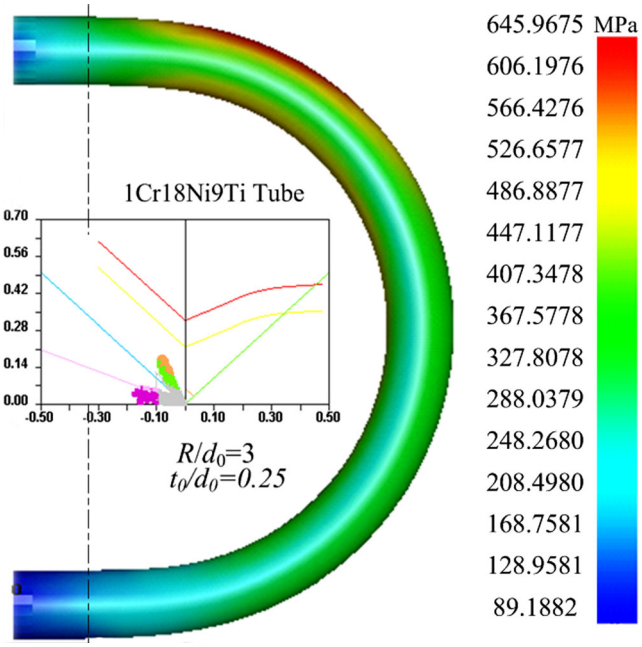

Fig. 2 The distribution of equivalent stress and FEM results of deformation

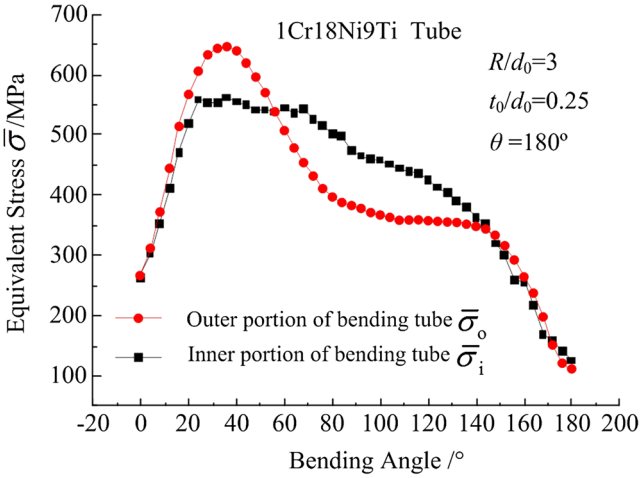

Fig. 3 The distribution of the maximum equivalent stress along the bending line (FEM result)

convex portion of tube $\overline{\sigma}_{\mathrm{o}}$ in the middle portion of tube shows a platform when decreasing. Though the deformation zone is in the loading state, it is still necessary to give the bending moment and the additional tensile force to the bent tube, for which the equivalent stress $\overline{\sigma}$ doesn't decrease to zero. The equivalent stress $\overline{\sigma}$ in the leading end and the terminating end decrease significantly due to the moderating effect of deformation and a certain amount of equivalent stress is also generated in the unbent portion of the tube. As the terminating end is near the instantaneous bending deformation zone which is still in loading state, the equivalent stress $\overline{\sigma}$ in the terminating end around the tangent point of the unbent tube and the bending die is always greater than that of the leading end.

If the axial tensile force is considered, the average equivalent stress $\overline{\sigma}$ in the outer convex portion of bending tube increases due to the increase of the total tangential tensile force, while the average equivalent stress $\overline{\sigma}$ in the inner concave portion of bending tube decrease due to the decrease of total deformation stress induced by the additional tensile force. As shown in Fig. 4, when the additional tensile force σ_{T} is equal to the yield stress of the tube σ_{s}, the average equivalent stress in the outer convex portion of bending tube is significantly greater than that in the inner concave, namely, $\overline{\sigma}_{\mathrm{o}} > \overline{\sigma}_{\mathrm{i}}$. The calculated curves of $\overline{\sigma}_{\mathrm{o}}$ agree well with the FEM results and show the similar variation tendency. While the additional tensile force is not considered, namely, $\sigma_{\mathrm{T}}=0$, the calculated curves of $\overline{\sigma}_{\mathrm{o}}$ significantly fall and the calculated curves of $\overline{\sigma}_{\mathrm{i}}$ rise, namely, $\overline{\sigma}_{\mathrm{o}} > \overline{\sigma}_{\mathrm{i}}$. It is important to note that approximate formula can only be used to calculate the average equivalent stress $\overline{\sigma}$, while the FEM results data $\overline{\sigma}$ is the maximum value. Actually when averaging the FEM results, we obtain $\overline{\sigma}_{\mathrm{i}} = 433.49\mathrm{MPa}$ and $\overline{\sigma}_{\mathrm{o}} = 430.84\mathrm{MPa}$, agreeing with the relation of the approximate calculation results, namely, $\overline{\sigma}_{\mathrm{i}} > \overline{\sigma}_{\mathrm{o}}$.

As the bending radius/diameter ratio R/d_0 decreases, the calculated results of $\overline{\sigma}$ and the simulation data all increase.

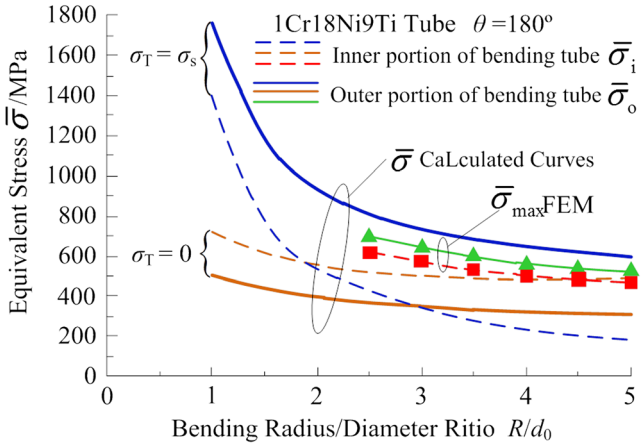

Fig. 4 The approximate calculation results of equivalent stress of the loading bending tube

When assuming $\sigma_T=\sigma_s$, the variation tendency of the FEM results agrees well with that of the experimental data, namely, the $\overline{\sigma}$ increases with the decreasing of R/d_0. While $\sigma_T=0$, the calculated curve of $\overline{\sigma}_i$ almost coincides with the FEM results. When $R/d_0\leq 2$, the calculated curves ($\sigma_T=\sigma_s$) increase rapidly with the decreasing of R/d_0. However, the calculated curves ($\sigma_T=0$) don't show the above variation tendency when $R/d_0\leq 2$. Actually, during the tube-bending testing and the industrial producing, the critical defects of crack or dent on tube wall would be induced by smaller R/d_0. Generally, $R/d_0=2$ is identified as the bending limit of the small coreless diameter tube.

4 The influence of the additional tensile fore on bending deformation

4.1 The displacement of the bending strain neutral layer

In pure bending, the stress neutral layer (NL) and the strain NL are kept moving toward the bending center under the function of bending moment to ensure that the stress and the strain are parallel to the bending plane [17]. If the additional tensile force is uniformly and independently applied in the tangential direction of the bending arc, the additional tensile force σ_T and the tangential stress induced by the bending moment must meet the static equilibrium relationship to keep the bending shape. It is assumed that the average wall thickness of the inner concave portion and the outer convex portion of bending tube separately are t_i and t_o. If there is no significant ovalization on the cross-section of the tube, the static equilibrium equations in the tangential direction of bending arc can be given as follows:

$$\int_0^{\pi}\left[\sigma_s\left(1-\frac{D}{E}\right)+\sigma_T+D\frac{r(\sin\varphi+\sin\alpha)}{R-r\sin\alpha}\right]r_m t_o d\varphi+\int_{\pi}^{\pi+\alpha}\left[\sigma_s\left(1-\frac{D}{E}\right)+\sigma_T+D\frac{r(\sin\varphi+\sin\alpha)}{R-r\sin\alpha}\right]r_m t_o d\varphi$$
$$+\int_{2\pi-\alpha}^{2\pi}\left[\sigma_s\left(1-\frac{D}{E}\right)+\sigma_T-D\frac{r(\sin\varphi+\sin\alpha)}{R-r\sin\alpha}\right]r_m t_o d\varphi+\int_{\pi+\alpha}^{2\pi-\alpha}\left[-\sigma_s\left(1-\frac{D}{E}\right)+\sigma_T+D\frac{r(\sin\varphi+\sin\alpha)}{R-r\sin\alpha}\right]r_m t_i d\varphi=0 \quad (21)$$

where r_m is the radius of the middle circle of the wall thickness.

According to large amount of experiment data and simulation results, the minimum wall thickness in the outer convex portion $t_{o\ min}$ gradually increases along the radial direction of the tube, changes to t_0 in the strain neutral layer, and finally changes to the maximum wall thickness in the inner concave portion of tube $t_{i\ max}$. Then, the average wall thickness of the inner concave and the outer convex portion of tube are expressed as follows

$$t_i=\frac{t_0+(t_0+\Delta t)}{2}=t_0+\frac{\Delta t}{2},\ t_o=\frac{t_0+(t_0-\Delta t)}{2}=t_0-\frac{\Delta t}{2} \quad (22)$$

Substituting Eq. 22 into Eq. 21 and integrating, the displacement angle related to the NL could be given approximately as follows:

$$|\alpha|=\frac{\frac{\pi}{2}\left[\frac{\sigma_T}{D}-\frac{\sigma_s}{D}\left(1-\frac{D}{E}\right)\frac{\Delta t}{t_0}\right](R/r-\sin\alpha)-\frac{\pi}{2}\sin\alpha+\frac{\Delta t}{t_0}\cos\alpha}{\left[\frac{\sigma_s}{D}\left(1-\frac{D}{E}\right)-\frac{\sigma_T\Delta t}{D\ t_0}\right](R/r-\sin\alpha)-\frac{\Delta t}{t_0}\sin\alpha} \quad (23)$$

If $\sigma_T=\sigma_s$, Eq. 23 can be simplified as follows:

$$\alpha=\frac{\frac{\pi}{2}\frac{\sigma_s}{D}\left[1-\left(1-\frac{D}{E}\right)\frac{\Delta t}{t_0}\right](R/r-\sin\alpha)-\frac{\pi}{2}\sin\alpha+\frac{\Delta t}{t_0}\cos\alpha}{\frac{\sigma_s}{D}\left[\left(1-\frac{D}{E}\right)-\frac{\Delta t}{t_0}\right](R/r-\sin\alpha)-\frac{\Delta t}{t_0}\sin\alpha} \quad (23a)$$

It is revealed that the displacement angle α related to the NL increases with the increase of the additional tensile force

σ_T and the displacement angle α related to the NL has definite function relation to the variation of wall thickness $\Delta t/t_0$. The displacement angle α related to the NL and the radius of the middle circle in the wall thickness r_m could be calculated by testing σ_T and $\Delta t/t_0$. When $\sigma_T=\sigma_s$ and the variation of wall thickness of tube is neglected, the displacement angle α related to the NL is calculated by numerical method, involving three different materials of 1Cr18Ni9Ti tube, 5A03 tube, and T2 tube. When $R/d_0=3$, the results respectively are as follows: $\alpha_{1Cr18Ni9Ti}=36.888°$, $\alpha_{5A03}=25.786°$, $\alpha_{T2}=19.939°$.

4.2 The influence of the additional tensile force on the wall thickness

In the NC tube bending, the additional tensile force aggravates the thinning of the outer wall of the tube and remits the thickening of the inner wall of the tube. Therefore, wrinkling rarely occurs in bending of thin-walled tubes with small diameter. The bending of thin-walled tubes with small diameter always fails due to the limited stiffness of the cross-section of the tube and the dent on tube wall before cracking [18]. Though the cracking in bending rarely happens, the quite smaller wall thickness decreases the stiffness in using and will induce the explosion in the conveying process of high-pressure fluid. Therefore, the related industrial application should be controlled and checked accurately.

Based on the assumption that the volume is uncompressible during bending, according to Eq. 6 and the plane strain relation, we can obtain the variation of wall thickness $\Delta t/t_0$ as the following:

$$\frac{\Delta t}{t_0}=\frac{1+\sin\alpha}{2R/d_0+2t_0/d_0-\sin\alpha} \tag{24}$$

From Eq. 24, it is shown that the variation of wall thickness $\Delta t/t_0$ and the bending radius/diameter ratio R/d_0 depend on the wall thickness/diameter ratio t_0/d_0 of tube. According to Fig. 5, it is revealed that the displacement angle α related to the NL accelerates the drawing deformation and induces the decrease of the wall thickness, namely, the greater the movement (α) of the NL, the more significant the growing of variation of wall thickness $\Delta t/t_0$. For the same α, the variation of wall thickness $\Delta t/t_0$ increases with the decrease of the bending radius/diameter ratio R/d_0 and the decrease of the wall thickness/diameter ratio t_0/d_0, but the variation of $\Delta t/t_0$ with R/d_0 is much greater than the variation of $\Delta t/t_0$ with t_0/d_0. It means that the bending radius/diameter ratio R/d_0 influences the variation of wall thickness more in the tube bending without mandrel.

According to the calculated curves, as the bending deformation becomes moderate with the increase of R/d_0, the growing tendency of $\Delta t/t_0$ becomes insignificant with the

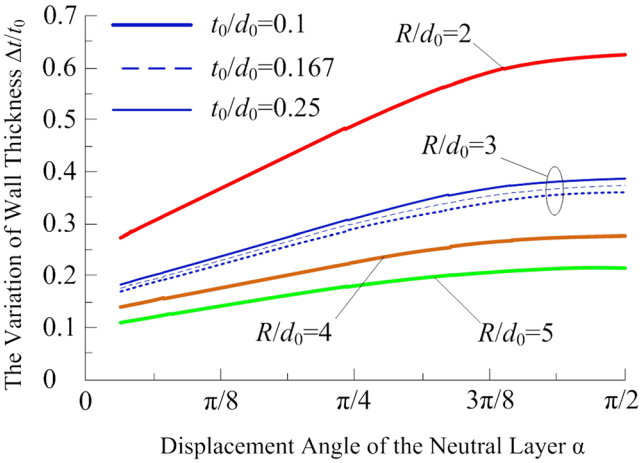

Fig. 5 The variation of wall thickness with the accreting of the movement of the NL

increase of the movement (α) of the NL. For smaller bending radius/diameter ratio R/d_0, the bending deformation accelerates more greatly and the greater the movement (α) of the NL, the more significant the growing tendency of $\Delta t/t_0$ is. When the NL moves to the inner concave surface of te tube where α is near π/2, $\Delta t/t_0$ does not vary with the increase of α anymore.

When the tangential strain and the radial strain are expressed by the true strain, based on the plane deformation relation, the variation of wall thickness $\Delta t/t_0$ could be expressed as the following:

$$\frac{\Delta t}{t_0}=\frac{1}{2t_0/d_0}\left[\left(\frac{1}{2}+\frac{R}{d_0}+\frac{t_0}{d_0}\right)-\sqrt{\left(\frac{1}{2}+\frac{R}{d_0}+\frac{t_0}{d_0}\right)^2-2\frac{t_0}{d_0}(1+\sin\alpha)}\right] \tag{25}$$

To learn the real situation of the distributions of wall thickness, the bending tubes in the experiment are bisected along the central layer of bending longitudinal direction and the wall thickness of different location is measured. As in Fig. 6, the wall thickness of the outer convex portion of tube is significantly smaller than that of the inner concave. Meanwhile, the wall thickness of the outer convex portion of tube is non-uniformly distributed. The significant increase and decrease of the wall thickness are all in the middle portion of the tube. The most significant wall thickness reduction is around the field where θ=30° near the bending terminating end, which is related to the maximum equivalent stress (FEM result) and the causation will be studied as important part of the following work.

To study the influence of the bending deformation condition on the approximate calculated results, the α calculated in certain deformation is substituted into the Eqs. 24 and 25. The calculated curve of the variation of $\Delta t/t_0$ with R/d_0 is shown in Fig. 7.in which some measuring results are concluded. From the curves, it is revealed that the calculated and the measured $\Delta t/t_0$ all decrease with the increase of R/d_0 and being

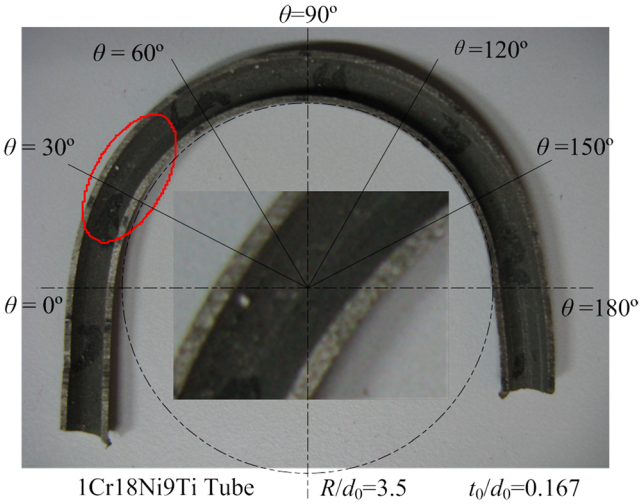

Fig. 6 The longitudinal profile of bending tube

compared with the nominal strain, the curves calculated by Eq. 25 with the true strain are more close to the measured results. In addition, if the displacement of the NL is neglected, the approximate calculation curves (α=0) are lower and more close to the measuring results. The calculated results of $\Delta t/t_0$ are relatively larger than the measuring results, indicating that there is some shortage in the approximate formula and it may be attributed to the ignorance of the cross-sectional ovalization and displacement of the bending tube.

4.3 The influence of additional tensile force on the shape of the cross section of the tube

In the NC tube-bending test, the inner concave portion of tube is restricted by the grooves of the bending die, and the outer radius remains unchanged. While the outer convex portion of tube is in contactless and free-deformation condition, the deformation and displacement in radial and circumferential direction of the outer convex portion of tube will be induced by the combined function of the bending moment and the additional tensile force, attributing to the ovalization of the

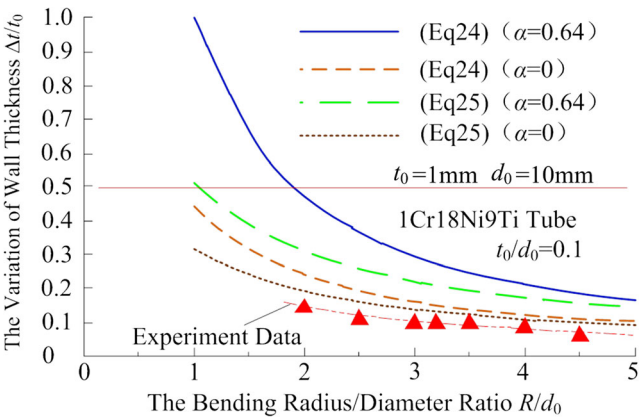

Fig. 7 The approximate calculation results and the FEM results of $\Delta t/t_0$

cross-section of the tube [19]. Figure 8a shows the simulation result of the distribution of the equivalent stress and the shape change of the cross-section of the tube. Fig. 8b shows the experimental result of the shape change of the cross-section of the tube, agreeing well with the simulation result in the ovalization of the cross-section of the tube in representative region. It is revealed that the ovalization deformation is mainly located in the middle portion of the tube, but the ovalization in the two end of the tube reduces due to the moderate deformation of the straight portion. The maximum equivalent stress in the inner concave portion of tube is discontinuous and the wrinkling tendency occurs in the inner concave portion of the tube. In the practical NC tube bending, the wrinkling rarely happens in thin-walled tubes with small diameter.

The ovalization deformation not only destroys the rigidity of the cross section of bending tube but also leads to the unpredictable pressure and flow pulsation in conveying process of high pressure fluid. The severe ovalization of the tube's inner contour is also the potential cause inducing the explosion in the conveying process of high-pressure fluid, which is necessary to be paid great attention in producing as same as the thinning of the tube wall. Based on the assumption of plane strain ε_φ=0, the thinning of the outer convex portion of tube is the most important factor influencing the outline shape of the tube. The ratio of the minor axis to the original radius of outer contour of bending tube φ_m can be expressed as

$$\varphi_m = \frac{d_0 - d_{\min}}{d_0} = \frac{\Delta t}{d_0} \tag{26}$$

According to the relation of Eq. 24 and 25, we could obtain the following:

$$\varphi_m = \frac{t_0}{d_0} \frac{1+\sin\alpha}{2R/d_0 + 2t_0/d_0 - \sin\alpha} \tag{27}$$

$$\varphi_m = \frac{1}{2}\left[\left(\frac{1}{2}+\frac{R}{d_0}+\frac{t_0}{d_0}\right) - \sqrt{\left(\frac{1}{2}+\frac{R}{d_0}+\frac{t_0}{d_0}\right)^2 - 2\frac{t_0}{d_0}(1+\sin\alpha)}\right] \tag{28}$$

Since the approximate calculation above is based on the plane strain assumption, besides the bending deformation conditions, the thinning of the tube wall and the displacement of the strain neutral layer are also important factor affecting the outer contour of the tube. As shown in Fig. 9, the calculated curves of φ_m is lower than the measured results but the variation tendency of the two results agree well. It means that when R/d_0>2 (the range of routine bending of thin-walled

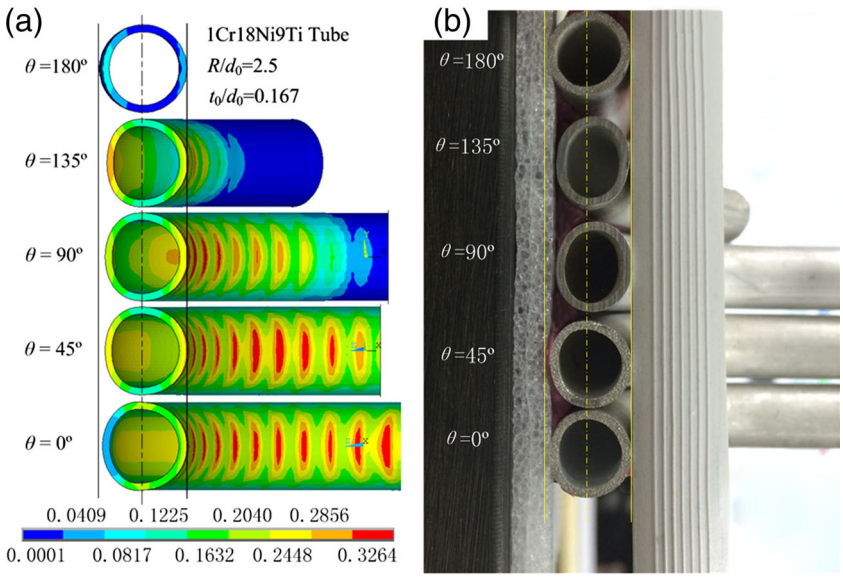

Fig. 8 The experimental results and FEM microtomy of the ovalization of the cross-section of the tube in representative region

coreless tubes with small diameter), the φ_m increases gradually as the decrease of the bending radius/diameter ratio R/d_0. However, in the case of R/d_0=2, the φ_m increases quite rapidly. In addition, the greater the wall thickness/diameter ratio t_0/d_0, the larger the calculated results of φ_m are. The conclusion above seems in conflict with the above-mentioned conclusion that $\Delta t/t_0$ decreases with the t_0/d_0 increasing. Then the Eq. 26 is adjusted as following:

$$\varphi_m = \frac{\Delta t}{t_0}\cdot\frac{t_0}{d_0} \tag{26a}$$

It is understandable that when the variation of wall thickness $\Delta t/t_0$ is unchanged, the increasing of t_0/d_0 means the decrease of d_0, which increases the value of φ_m

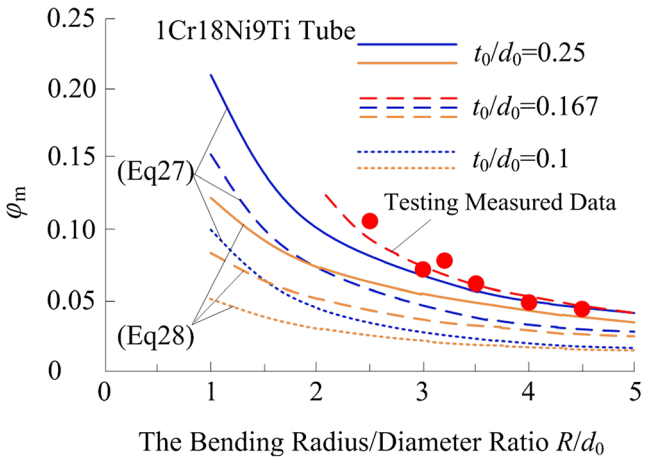

Fig. 9 The approximate calculated results and the testing measured results of φ_m

5 The control of the additional tensile force

It is revealed from theabove analysis that proper control of the additional tensile force can reduce the thinning of the bending tube's wall and the ovalization of the cross-section of the tube. For the linear hardening material model, when the stress state in tangential direction is only considered, the total outer tangential tensile force should be smaller than the ultimate tensile strength of material [20, 21]. Namely, when $\sigma_T \le \sigma_s$, we obtain the following:

$$\sigma_b \ge \sigma_s + \sigma_T + D(\varepsilon_\theta - \varepsilon_s - \varepsilon_{\theta T}) = (\sigma_s + \sigma_T)\left(1-\frac{D}{E}\right) + D\frac{r_o + r\sin\alpha}{R - r\sin\alpha} \tag{29}$$

Substituting the equation of original outer radius of tube r_o, namely, $r_o = r_0 - \Delta t$, we can obtain the allowable tangential additional tensile stress as the following:

$$[\sigma_T] \le \frac{1}{1-D/E}\left[\sigma_b - \frac{D}{2R/d_0 - \sin\alpha}\left(1 - 2\frac{\Delta t}{t_0}\frac{t_0}{d_0} + \sin\alpha\right)\right] - \sigma_s \tag{30}$$

If the thinning of the outer convex portion of tube and the possible radial displacement are neglected, it is approximatively considered that $r_o = r_0$, the Eq. 30 can be simplified as

$$[\sigma_T] \le \frac{1}{1-D/E}\left(\sigma_b - D\frac{1+\sin\alpha}{2R/d_0 - \sin\alpha}\right) - \sigma_s \tag{31}$$

The above equation provides significant reference for the design of NC tube bender and the NC tube-bending techniques, namely, the additional tensile force should be less than the above value in Eq. 31. Otherwise, the bigger value of σ_T will lead to the severe thinning of the tube wall and even the crack. To simplify the calculation, we substitute the equation

α=0.64 into Eq. 31 and obtain the curves in Fig. 10. It is shown that the allowable tangential additional tensile stress $[\sigma_T]$ increases with the increase of R/d_0. For T2 tube and 5A03 tube, when $R/d_0>2$ (the range of routine bending of thin-walled coreless tubes with small diameter), the $[\sigma_T]$ could be larger than the initial yield strength σ_s, while for 1Cr18Ni9Ti tube, only when $R/d_0>3$, the $[\sigma_T]$ is allowed to be larger than σ_s.

If the engineering allowable value of variation of wall thickness $\Delta t/t_0$ is substituted into Eq. 30, the obtained value of $[\sigma_T]$ is a little larger but almost coincides with the calculated curves in above coordinates, indicating that it is inappropriate to enlarge the additional tensile force in the allowable range of the variation of tube's wall thickness. Especially for the bending deformation conditions of smaller R/d_0, the additional tensile force should be reduced as much as possible.

when $R/d_0=2$, for 1Cr18Ni9Ti tube, the calculated additional tensile force has the following relation, namely, $[\sigma_T]\le 0$, indicating that it is no more allowable to apply additional tensile force on the tube. It is also one of the main reasons for the principle that the limit bending radius/diameter ratio $R/d_0\approx 2$ in conventional coreless bending of smaller diameter and thin wall thickness tubes. In the real bending production, it is more likely to utilize the push bending or the other bending methods when $R/d_0\le 2$.

According to the above analysis, the maximum allowable additional tensile force can be derived as follows:

$$[T]\le\left[\frac{1}{1-D/E}\left(\sigma_b-D\frac{1-\Delta t/r+\sin\alpha}{2R/d_0-\sin\alpha}\right)-\sigma_s\right]\pi d_0 t_0\left(1-\frac{t_0}{d_0}\right) \tag{32}$$

If the thinning of the outer convex portion of tube is neglected, Eq. 32 can be simplified as follows:

$$[T]\le\left[\frac{1}{1-D/E}\left(\sigma_b-D\frac{1+\sin\alpha}{2R/d_0-\sin\alpha}\right)-\sigma_s\right]\pi d_0 t_0\left(1-\frac{t_0}{d_0}\right) \tag{32a}$$

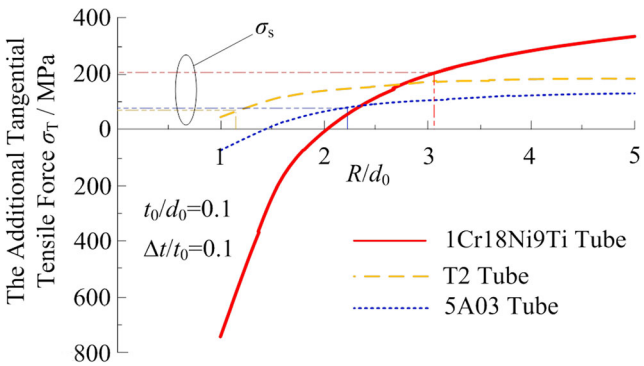

Fig. 10 The relation of the allowable additional tensile stress with the bending radius/diameter ratio R/d_0

The meaning of the above equation is that the sliding friction between the surface of tube wall and the grooves of the pressure die and the wiper die must be considered in the design, debugging, using of NC tube bender, and the process of NC tube bending. The excessive friction between the surface of tube wall and the grooves of the pressure die may enlarge the additional tensile force and lead to the severe thinning of the tube wall and even the crack.

Therefore, the roughness of working surface of the grooves should be reduced and the lubrication problem should be taken into consideration according to the specific bending deformation situation.

6 Conclusions

(1) The formulas are derived to calculate the average principal stress and the equivalent stress in different directions of the bending tube surface. The average equivalent stress is close to the FEM result and the variation tendency of the average equivalent stress agrees well with the experimental data. The FEM results show that the equivalent stress is non-uniformly distributed along the longitudinal direction of bending tube. The maximum equivalent stress is localized at the field around the terminating and the equivalent stress reduces gradually when close to the two end of the tube due to the moderate deformation of the straight portion. The equivalent stress of the terminating end is larger than that of the leading end.

(2) In the NC tube bending, the additional tensile force enlarges the displacement of the strain NL, reduces the thickening of the wall of the inner concave portion of tube, and accelerates the thinning of the outer convex portion of tube. The calculated results of the variation of wall thickness $\Delta t/t_0$ are close to the FEM experimental data, and the calculation accuracy of the formulas derived by using the true stress is relatively higher. By analysis, it is believed that the calculation deviation is attributed to the deformation and displacement of the cross-section of the tube in circumferential direction.

(3) The thickening of the wall in inner concave portion of tube and the thinning of the wall in outer convex portion of tube lead to the ovalization of tube's inner and outer contour, not only destroying the rigidity of the cross section of bending tube but also inducing the unpredictable pressure and flow pulsation in conveying process of high-pressure fluid. The ratio of the minor axis to the original radius of outer contour of bending tube is a little lower than that of the experimental data. But, the variation tendency is similar that the φ_m increases with the decrease of the bending radius/diameter ratio R/d_0.

(4) The approximate calculation and analysis show that the additional tensile force must be controlled to avoid the collapsing and the crack of the tube's wall attributed to the extreme thinning of the tube wall and the worse ratio of the minor axis to the original radius of outer contour of bending tube. In addition, it is suggested that the roughness of working surface of the grooves should be reduced and the lubrication problem should be taken into consideration to indirectly control the additional tensile force.

References

1. Guan YJ, Yuan GP, Sun S, Zhao GQ (2012) Process simulation and optimization of laser tube bending. Int J Adv Manuf Technol 65:333–342
2. Huang YM, Huang YM (2002) Influence of punch radius and angle on the outward curling process of tubes. Int J Adv Manuf Technol 19: 587–596
3. Liu KX, Liu YL, Yang H (2013) Experimental study on the effect of dies on wall thickness distribution in NC bending of thin-walled rectangular 3A21 aluminum alloy tube. Int J Adv Manuf Technol 68:1867–1874
4. Kim YJ, Kim JH (2008) Effects of local wall thinning on plastic limit loads of elbows using geometrically linear FE limit analyses. Eng Fract Mech 75:2225–2245
5. Murata M, Kuboki T, Takahashi K, Goodarzi M, Jin Y (2008) Effect of hardening exponent on tube bending. J Mater Process Technol 201:189–192
6. Zhao GY, Liu YL, Yang H (2010) Effect of clearance on wrinkling of thin-walled rectangular tube in rotary draw bending process. Int J Adv Manuf Technol 50:85–92
7. Liu YC, Michael LD (2008) Bending collapse of thin-walled circular tubes and computational application. Thin-Walled Struct 46:442–450
8. Oliveira A, Worswick MJ (2009) Tube bending and hydroforming of aluminium alloy S-rails. Int J Mater Form 2:197–215
9. Strano M (2005) Automatic tooling design for rotary draw bending of tubes. Int J Adv Manuf Technol 26:733–740
10. Li H, Yang H (2009) Numerical study on deformation behaviors of thin-walled tube NC bending with large diameter and small bending radius. Comput Mater Sci 45:921–934
11. Zhan M, Huang T, Jiang ZQ, Zhang PP, Yang H (2013) Determination of process parameters for the NC bending of a TA18 tube. Int J Adv Manuf Technol 68:663–672
12. Zhang ZY, Yang H, Li H, Ren N, Tian YL (2011) Bending behaviors of large diameter thin-walled CP-Ti tube in rotary draw bending. Mater Int 21:401–412
13. Da-xin E, He HH, Liu XY (2009) Experimental study and finite element analysis of spring-back deformation in tube bending. Int J Mineral Metall Mater 2:177–183
14. Daxin E, Liu YF (2008) Springback and time-dependent springback of 1Cr18Ni9Ti stainless steel tubes under bending. Mater Des 31: 1256–1261
15. Daxin E, Chen MF (2010) Numerical solution of thin-walled tube beding spingback with exponential hardening law. Steel Res Int 81: 286–291
16. Daxin E, Liu YF, Feng HB (2010) Deformation analysis for the rotary draw bending process of circular tubes: stress distribution and wall thinning. Steel Res Int 81:1084–1088
17. Liu YF, Daxin E (2011) Effects of cross-sectional ovalization on springback and strain distribution of circular tubes under bending. J Mater Eng Perform 20:1591–1599
18. Daxin E, Guan ZP, Chen JS (2012) Influence of additional tensile force on springback of tube under rotary draw bending. J Mater Eng Perform 21:2316–2322
19. Daxin E, Chen JS, Ding J (2012) In-plane strain solution of stress and defects of tube bending with exponential hardening law. Mech Based Des Struct Mach 40:257–276
20. Daxin E, Chen JS, Yang C (2013) Plane strain solution and cross-section flattening analysis in tube bending with linear hardening law. J Strain Anal 48:198–211
21. Daxin E, Chen JS, Zhang JW (2013) Effects of process parameters on wrinkling of thin-walled circular tube under rotary draw bending. Int J Adv Manuf Technol 68:1505–1516